

An Investigation of Charm Quark Jet Spectrum and Shape Modifications in Au+Au Collisions at $\sqrt{s_{\text{NN}}} = 200$ GeV*

DIPTANIL ROY (*STAR Collaboration*)
ROYDIPTANIL@GMAIL.COM

Rutgers University

Received July 27, 2022

1 Partons in heavy-ion collisions interact strongly with the Quark-Gluon
2 Plasma (QGP), and hence have their energy and shower structure modi-
3 fied compared to those in vacuum. Theoretical calculations predict that
4 the radiative energy loss, which is the dominant mode of energy loss for
5 gluons and light quarks in the QGP, is suppressed for heavy quarks at low
6 transverse momenta (p_{T}). At RHIC energies, lower energy jets closer to the
7 charm quark mass are more accessible, and could provide key insight into
8 the understanding of the mass dependence of parton energy loss. We re-
9 port the first measurements of the $D^0(c\bar{u})$ meson tagged jet p_{T} spectra and
10 the D^0 meson radial profile in jets reconstructed from Au+Au collisions at
11 $\sqrt{s_{\text{NN}}} = 200$ GeV, collected by the STAR experiment.

12 1. Introduction

13 Relativistic heavy-ion collisions produce Quark-Gluon Plasma (QGP),
14 as predicted by Quantum Chromodynamics (QCD) [1]. Internal probes
15 involving hard scattering processes are used to study the properties of the
16 QGP medium. Jets, one of such probes, manifest as a collimated cluster of
17 final state particles in the detector. The partons which give rise to these
18 jets lose energy to the QGP medium, either through collisions, or through
19 induced gluon *bremsstrahlung* - a phenomenon known as jet quenching [2].
20 The effects of jet quenching can be seen in measurements of inclusive jets
21 yield suppression [3] and modifications to the jet structure [4]. A study of
22 heavy flavor tagged jets can shed light on the mass and flavor dependence
23 of the parton energy loss and jet structure modifications. The dead-cone
24 effect [5], as predicted by the QCD, was measured for charm quarks in
25 pp collisions at the LHC [6], but remains elusive for heavy-ion collisions.

* Presented at Quark Matter 2022. This material is based upon work supported by the National Science Foundation under Grant No. 1913624.

Heavy flavor jets at the LHC have also yet to reveal significant differences with their inclusive counterparts [7, 8], possibly due to having energies much higher than the parton masses. Such studies at the RHIC energies, where lower energy jets are produced, could be the key to better understanding the parton mass dependence of the energy loss. This proceeding will focus on the first measurements of $D^0(\bar{D}^0)$ meson tagged jet transverse momentum (p_T) spectra and the $D^0(\bar{D}^0)$ meson radial profile in tagged jets from Au+Au collisions at $\sqrt{s_{NN}} = 200$ GeV.

2. Analysis Setup

This work uses Minimum Bias (MB) triggered Au+Au collision events at $\sqrt{s_{NN}} = 200$ GeV, collected in 2014 by the STAR detector [9] at RHIC. Events and tracks which pass standard quality cuts at STAR [10], are chosen within the pseudorapidity acceptance of $|\eta| < 1$. The analysis is done in three centrality bins: 0-10% (central), 10-40% (mid-central), and 40-80% (peripheral). $D^0(\bar{D}^0)$ mesons are reconstructed via the hadronic decay channel $D^0 \rightarrow K^- + \pi^+$ (and its charge conjugate) with a branching ratio of 3.89 % [11]. Several topological selections based on the decay geometry of $D^0(\bar{D}^0)$ are applied to the combinatorial $K\pi$ pairs in an event by using the Heavy Flavor Tracker (HFT) [12], which improves the resolution of tracking from 1 mm at Time Projection Chamber (TPC) to about 30 μm . A more thorough discussion on the selection criteria for the $D^0(\bar{D}^0)$ candidates is available in Ref. [13].

Full jets are reconstructed from TPC tracks and electromagnetic calorimeter (ECAL) towers with $p_T > 0.2$ GeV/ c , and transverse energy $E_T > 0.2$ GeV respectively. The jets are defined using the anti- k_T clustering algorithm available in the FastJet package [14], with a radius parameter of $R = 0.4$ in the $\eta - \phi$ space, and are selected in the pseudorapidity range $\eta_{\text{jet}} = 1 - R$. The K and π daughter tracks are replaced with the corresponding $D^0(\bar{D}^0)$ candidate before the jets are reconstructed. A jet area based background subtraction is applied to minimize the effect of the soft background on the jets [15]. Jets with a $D^0(\bar{D}^0)$ constituent with $p_{T,D^0} \in (5, 10)$ GeV/ c are considered as a D^0 tagged jet for this analysis.

3. $D^0(\bar{D}^0)$ Jet Spectra and Shape Modifications

To extract the raw yield of $D^0(\bar{D}^0)$ mesons, a method called $sPlot$ [16] is used. $sPlot$ calculates per event weights, called sWeights, from an unbinned likelihood fit to the $D^0(\bar{D}^0)$ invariant mass distribution over all kinematics. The weights classify how ‘*signal-like*’ a $D^0(\bar{D}^0)$ candidate is. Fig. 1 shows the invariant mass distribution of $K\pi$ candidates in the p_T region of

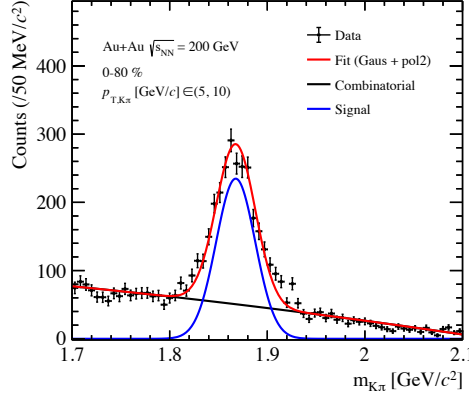


Fig. 1. The invariant mass distribution of $K\pi$ pairs with $p_T \in (5, 10)$ GeV/c. The unlike sign $K\pi$ pairs distribution (*black*) is fit with a Gaussian plus second-order polynomial (*red*) to estimate the $D^0(\bar{D}^0)$ yield. The signal after the removal of the background (*blue*) is also shown on the same scale.

5–10 GeV/c for 0–80% MB events. The invariant yield of $D^0(\bar{D}^0)$ tagged jets is represented by the formula:

$$\frac{d^2 N_{\text{jet}}}{2\pi N_{\text{evt}} p_{T,\text{jet}} dp_{T,\text{jet}} d\eta} = \frac{1}{\text{B.R.}} \times \frac{N_{\text{jet}}^{\text{raw}}}{2\pi N_{\text{evt}} p_{T,\text{jet}} \Delta p_{T,\text{jet}} \Delta \eta} \times \frac{1}{\epsilon_{\text{corr}}} \quad (1)$$

where B.R. is the $D^0 \rightarrow K^-\pi^+$ decay branching ratio ($3.89 \pm 0.04\%$), $N_{\text{jet}}^{\text{raw}}$ is the reconstructed $D^0(\bar{D}^0)$ tagged jets raw counts, and N_{evt} is the total numbers of events used in this analysis. The raw yields are corrected for the tracking efficiencies and acceptances of the TPC and HFT, topological cut efficiency, particle identification efficiency, and finite vertex resolution based on the correction factors derived in Ref. [13], and the total correction factor is ϵ_{corr} . The nuclear modification factor R_{CP} is defined as the ratio of $\langle N_{\text{coll}} \rangle$ -normalized yields between central and peripheral collisions, where $\langle N_{\text{coll}} \rangle$ is the average number of the binary collisions for a centrality class.

The radial distribution of $D^0(\bar{D}^0)$ mesons in tagged jets is defined by the formula:

$$\frac{1}{N_{\text{jet}}} \frac{dN_{\text{jet}}}{dr} = \frac{1}{N_{\text{jet}}} \frac{N_{\text{jet}}|_{\Delta r}}{\Delta r} \quad (2)$$

where $r = \sqrt{(\eta_{\text{jet}} - \eta_{D^0})^2 + (\phi_{\text{jet}} - \phi_{D^0})^2}$ is the distance of the $D^0(\eta_{D^0}, \phi_{D^0})$ from the jet axis $(\eta_{\text{jet}}, \phi_{\text{jet}})$ in the $\eta - \phi$ plane, and $N_{\text{jet}}|_{\Delta r}$ is the number of jets with $D^0(\bar{D}^0)$ mesons in the Δr interval.

A Bayesian unfolding procedure [17], with a Monte-Carlo (MC) generated event sample, is used to account for the detector inefficiencies in

jet reconstruction. A $D^0(\bar{D}^0)$ -enriched sample of pp collision events at $\sqrt{s} = 200$ GeV is generated using PYTHIA v8.303, with the ‘Detroit’ tune [18], and propagated through the STAR detector using the GEANT3 [19] package. The FONLL (Fixed Order + Next-to-Leading Logarithms) [20] charm quark spectrum is used as a prior for the unfolding procedure. The charm jet fragmentation function is modeled using PYTHIA, and a systematic study of effects of its variation is in the works. Observables with an asterisk(*), found later in this proceeding, are corrected with the PYTHIA fragmentation function. The fluctuation due to the heavy-ion background is estimated by embedding one ‘single-particle’ jet each in MB Au+Au events, and then matching each embedded jet with a reconstructed jet containing the tagged ‘single-particle’. The quantity $\Delta p_{T,SPjet} = p_{T,SPjet}^{\text{det}} - p_{T,SPjet}^{\text{part}}$ models this fluctuation. The superscript ‘part’ refers to particle-level jets, and ‘det’ refers to detector-level jets. For the D^0 meson radial profile, the aforementioned Bayesian unfolding procedure is used to simultaneously correct N_{jet} as a function of $p_{T,jet}$ and Δr .

The systematic uncertainties across the bins in the reported observables are dominated by the following contributions: a) differences in the invariant yield of D^0 mesons calculated using the *sPlot* method, and a like-sign background subtraction method, and b) systematic uncertainty in $D^0(\bar{D}^0)$ reconstruction taken from Ref. [13]. Systematic variations related to the unfolding procedure are estimated by varying the following: a) the prior from FONLL to the jet distribution for D^0 tagged jets in pp collisions at $\sqrt{s} = 200$ GeV generated by PYTHIA, and b) the regularisation parameter.

The efficiency-corrected invariant yield of $D^0(\bar{D}^0)$ jets is shown in the left panel of Fig. 2 for $p_{T,D^0} \in (5, 10)$ GeV/ c , as a function of $p_{T,jet}$ in 0-10%, 10-40%, and 40-80% Au+Au collisions. The spectra in the first two centrality bins are scaled by arbitrary factors for better visibility. The nuclear modification factor R_{CP}^* for the central and the mid-central Au+Au collisions are shown in the right panel of Fig. 2, with the peripheral centrality bin as the reference. The bands (blue and green) are uncertainties associated with $\langle N_{coll} \rangle$. The D^0 jet R_{CP}^* shows a stronger suppression in central collisions than in mid-central collisions at low $p_{T,jet}$. R_{CP}^* also shows an increasing trend with $p_{T,jet}$ for both centrality bins. This trend is qualitatively different from the R_{CP} measured for inclusive jets at RHIC [3].

The radial profile for $D^0(\bar{D}^0)$ mesons with $p_{T,D^0} \in (5, 10)$ GeV/ c in the tagged jets is shown as a function of the distance from the jet axis (r) in 0-10%, 10-40%, and 40-80% Au+Au collisions in the left panel of Fig. 3. The ratio of the radial profiles for the central and mid-central events with peripheral events, shown in the right panel of Fig. 3, is found to be consistent with unity within the uncertainties. The large uncertainties are dominated by the limited statistics in the peripheral centrality bin.

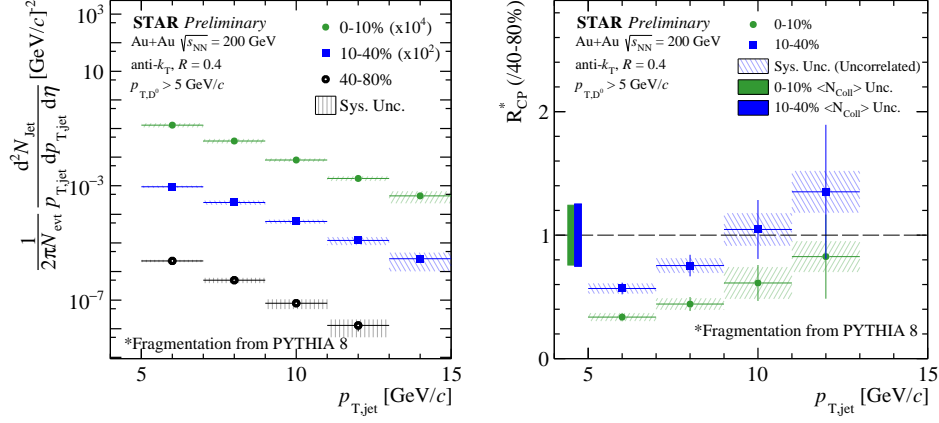


Fig. 2. **Left:** $D^0(\bar{D}^0)$ tagged jets p_T spectra with $p_{T,D^0} \in (5, 10)$ GeV/c in different centrality classes; **Right:** Nuclear modification factor R_{CP}^* for D^0 jets.

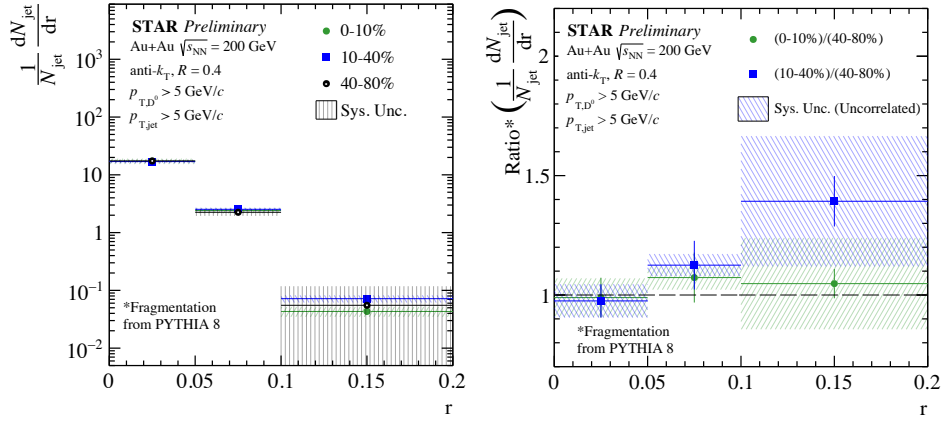


Fig. 3. **Left:** D^0 radial profile for $D^0(\bar{D}^0)$ tagged jets with $p_{T,D^0} \in (5, 10)$ GeV/c in different centrality classes; **Right:** Ratio of D^0 radial profiles for central and mid-central events with respect to D^0 radial profile for peripheral events.

4. Discussion

In this proceeding, the first measurements of D^0 meson tagged jet p_T spectra and D^0 meson radial profile are reported for $p_{T,D^0} \in (5, 10)$ GeV/c in Au+Au collisions at $\sqrt{s_{NN}} = 200$ GeV. The D^0 $p_{T,jet}$ spectra is found to be suppressed for central and mid-central collisions at low $p_{T,jet}$ with the nuclear modification factor showing an increasing trend with $p_{T,jet}$. This

130 trend is qualitatively different from the inclusive jet measurements at RHIC.
 131 The radial profile of $D^0(\bar{D}^0)$ in its tagged jets is found to be consistent for
 132 different centralities. Within the current uncertainties, no hint of differences
 133 in charm quark diffusion is observed in the presence of the QGP medium.
 134 Further studies are ongoing to extend our measurements to lower p_{T,D^0}
 135 allowing us to get closer to the charm quark mass. These measurements
 136 can constrain theoretical models on parton flavor and mass dependencies of
 137 jet energy loss.

138 REFERENCES

- 139 [1] STAR Collaboration. *Nuclear Physics A*, 757(1-2):102–183, 2005.
- 140 [2] Megan Connors *et al.* *Rev. Mod. Phys.*, 90:025005, 2018.
- 141 [3] STAR Collaboration. *Phys. Rev. C*, 102:054913, 2020.
- 142 [4] CMS Collaboration. *Physics Letters B*, 730:243–263, 2014.
- 143 [5] Yu L Dokshitzer *et al.* *J. Phys. G: Nucl. Part. Phys.*, 17(10):1602–1604,
 144 1991.
- 145 [6] ALICE Collaboration. *Nature*, 605(7910):440–446, 2022.
- 146 [7] CMS Collaboration. *Phys. Rev. Lett.*, 113:132301, 2014.
- 147 [8] CMS Collaboration. *Phys. Rev. Lett.*, 125:102001, 2020.
- 148 [9] STAR Collaboration. *Nuc. Ins. Methods. A*, 499(2):624–632, 2003.
- 149 [10] STAR Collaboration. *Phys. Rev. Lett.*, 119:062301, 2017.
- 150 [11] Particle Data Group. *Prog. Theor. Exp. Phys*, 2020:083C–84, 2020.
- 151 [12] L. Greiner *et al.* *Nuc. Ins. Methods. A*, 650(1):68–72, 2011.
- 152 [13] STAR Collaboration. *Phys. Rev. C*, 99:034908, 2019.
- 153 [14] Matteo Cacciari *et al.* *The Eur. Phys. Jour. C*, 72(3):1896, 2012.
- 154 [15] Matteo Cacciari *et al.* *Physics Letters B*, 659(1):119–126, 2008.
- 155 [16] M. Pivk *et al.* *Nuc. Ins. Methods. A*, 555(1):356–369, 2005.
- 156 [17] G. D’Agostini. *Nuc. Ins. Methods. A*, 362(2):487–498, 1995.
- 157 [18] Manny Rosales Aguilar and *et al.* *arXiv*, 2021.
- 158 [19] R. Brun and *et al.* *CERN-DD-EE-84-1*, 1987.
- 159 [20] M. Cacciari *et al.* *JHEP*, 1998(05):007–007, 1998.